PHYSICAL REVIEW D **88,** 073001 (2013)

Thunderstorm ground enhancements: Gamma ray differential energy spectra

A. Chilingarian, G. Hovsepyan, and L. Kozliner
Yerevan Physics Institute, Alikhanyan Brothers 2, Yerevan 0036, Armenia
(Received 8 July 2013; published 1 October 2013)

The shape and evolution of the energy spectra of the thunderstorm ground enhancement (TGE) electrons and gamma rays shed light on the origin of TGEs, on the relationship of modification of the energy spectra (MOS) and relativistic runaway electron avalanche processes, on the nature of the seed particles, and on the strength and elongation of an atmospheric electric field. However, till now the measurements of energy spectra of TGE electrons and gamma rays have been rather scarce. For the first time, we present differential energy spectra of gamma rays in the wide energy range 4–100 MeV for five TGE events detected in 2012–2013 at Aragats. We use the special technique of electron/gamma ray fraction determination to select TGE events with very small contamination of electrons. The network of large NaI spectrometers located 3200 m above sea level measured energy spectra of gamma rays. The power law indices of ''small'' TGEs are rather close to the background cosmic gamma ray spectrum ($\gamma \sim -2$); thus, we may deduce that these small events are due to MOS of cosmic ray electrons in the electric field of a thundercloud. Larger TGEs measured by the NaI network and the two largest TGE events earlier recovered from energy releases in a 60-cm-thick scintillator have much steeper energy spectra typical for the avalanche process in atmosphere. The classification of TGEs according to intensity and gamma ray spectral index pointed toward two main mechanisms of the TGE gamma ray origin: the runaway process and modification of electron energy spectra in the thunderstorm atmospheres.

DOI: 10.1103/PhysRevD.88.073001 PACS numbers: 92.60.Pw, 13.40.−f, 94.05.Dd, 96.50.sb

I. INTRODUCTION

The boost of the secondary cosmic ray (CR) flux observed during thunderstorms, so-called thunderstorm ground enhancements (TGEs) [1,2], is the manifestation of high-energy processes in the terrestrial atmosphere [3]. The origin of TGEs is the strong electrical field in the thundercloud, giving rise to rather complicated physical phenomena, including at least six physical processes:

(1) Relativistic runaway electron avalanches (RREA) [4–8];
(2) Modification of the secondary cosmic ray (electrons, muons, protons and charged mesons) energy spectra [9–12];
(3) Photonuclear reactions of gamma rays [13–16];
(4) Attenuation of the cosmic ray muon flux [1,17];
(5) Roentgen and gamma radiation from the lightning [18];
(6) Prolonged (2–3 hours and more) enhancement of the low-energy (1–3 MeV) cosmic ray flux [19].

Starting in 2008, experimental facilities of the Aragats Space Environmental Center (ASEC) [20,21] have routinely measured time series and energy spectra of secondary cosmic ray fluxes. During these years, several new particle detectors were designed and fabricated, having a lower energy threshold and the ability to distinguish charged and neutral fluxes [22,23]. The variety of ASEC particle detectors allows us for the first time to detect RREA process in the atmosphere [2], recover both the electron and gamma ray energy spectra of the largest TGEs, and develop the model of the TGE process [12]. The statistical analysis of more than 300 TGE events, including TGE seasonal and daytime distributions, TGE amplitude, and duration graphs, are presented in [24]; the time series of hundreds of particle-measuring channels can be assessed online using multivariate visualization code ADEI [25] following the link http://crd.yerphi.am/ADEI.

The shape and evolution of the energy spectra of the TGE electrons and gamma rays shed light on the origin of TGE, on the relationship of MOS and RREA processes, on the nature of the seed particles, and on the strength and elongation of atmospheric electric field. However, till now the precise measurements of energy spectra of TGE electrons and gamma rays are rather scarce. The available gamma ray energy spectra measured with detectors located on Earth's surface [8,15,26–28] and in near space[1] [30,31] are based on rather small statistics and usually are averaged over many events. The variety and large sizes of ASEC detectors allow precise measurements of the gamma ray differential energy spectra of individual TGE events. Solving the inverse problem and ''unfolding'' the gamma ray spectra by multiple solutions of the direct problem, we estimate the electron integral spectra and gamma ray differential spectra of the two largest TGE events on September 19, 2009, and October 4, 2010 (see details in [12]). The energy deposit spectra measured by the 60–cm-thick plastic scintillators of the ASNT detector were used for recovering the gamma ray differential energy spectra

[1]Cumulative gamma ray energy spectra of so-called terrestrial gamma flashes (TGFs) [29].

(see details in [1]). The energy deposits of gamma rays incident on the 60-cm-thick scintillators located in the lightproof housings overviewed by photomultipliers were digitized and spectra were stored each minute. Assuming the analytic form of the possible RREA gamma ray spectra (power, exponential, or power with exponential cutoff), we tune free parameters (number of gamma rays fallen on the roof and spectral indices) by minimizing the "quality" function describing the closeness of deposit spectra simulated with GEANT code to the experimentally measured ones. Gamma rays were traced through the material of the roof above the detector and trough of the detector itself.

However, the length of 1.5 radiation lengths only is not enough to unambiguously measure gamma ray energy. The network of "deep" NaI crystals (12.5 cm thickness, ~5.2 radiation lengths) used for energy spectra measurement in a current study allows direct measurements of the gamma ray energy and estimation of the energy spectra without indirect methods of solving the inverse problem. For the first time, we present differential energy spectra of gamma rays in a wide energy range 4–100 MeV for five TGE events detected in 2012–2013 at Aragats. We use a special technique to select TGE events with very small contamination of electrons. Depending on the location of the thundercloud above the particle detectors, the relative fraction of the TGE electrons and gamma rays reaching the detector changes. Usually gamma rays are abundant due to much stronger attenuation of the electrons in the atmosphere; though we detect several "electron" TGEs [32], signaling that under some conditions, not yet fully understood, the electron flux can be prevailing. In the present paper, our goal is to investigate TGE gamma ray energy spectra for getting insight into their origin and for calibration of the ASEC particle detectors.

In the second section of the paper we present the technique of TGE event selection and detector output simulation. In Secs. III and IV, we describe the method of the electron/gamma ray ratio estimation. In the fifth section, we present measured gamma ray spectra. In Sec. VI, we calibrate the ASEC particle detectors by the integral gamma ray energy spectrum and in the conclusion we discuss the origin of the TGE events.

II. TGE DETECTION AND DETECTOR SIMULATION

On June 19, 2013, all particle detectors of the Aragats Space Environmental Center registered large thunderstorm ground enhancement. The Aragats multidirectional muon monitor (AMMM), the detector having a minimal relative error (RE) of 1-minute time series, consists of twenty-nine 1-m^2, 5-cm-thick scintillators, placed in lightproof iron boxes. A light capture cone and photomultiplier tubes are located on the top of each scintillator. On June 19, only 20 of 29 scintillators were operational. The large area of the detector provides maximal sensitivity to low-energy gamma rays and electrons of TGE. The relative error of the AMMM detector is ~0.1% for 1-minute time series.

The TGE was uncommonly lengthy (~1 hour, 7:00–8:00, with a maximum at 7:40); usually, TGE duration did not exceed 20 minutes (see [24]). As we see in Fig. 1, disturbance of the near-surface electric field starting at 7:00 originated a rise in particle flux. At 7:30, the electric field reached a value of -27 kV/m and stayed in the high negative domain till 7:52 (the minimum of field, -31 kV/m, was reached at 7:43). Simultaneously, the particle flux reached peak at 7:40 and consequently attenuated at 7:52 with the decay of the negative near-surface electric field. At the peak flux, there were 88,000 additional particles detected; the background value of cosmic ray flux was $1,020,000 +/- 1048$ particles per minute. Flux enhancement of 8.6% corresponds to 86 standard deviations from mean value. Other ASEC detectors also detected the

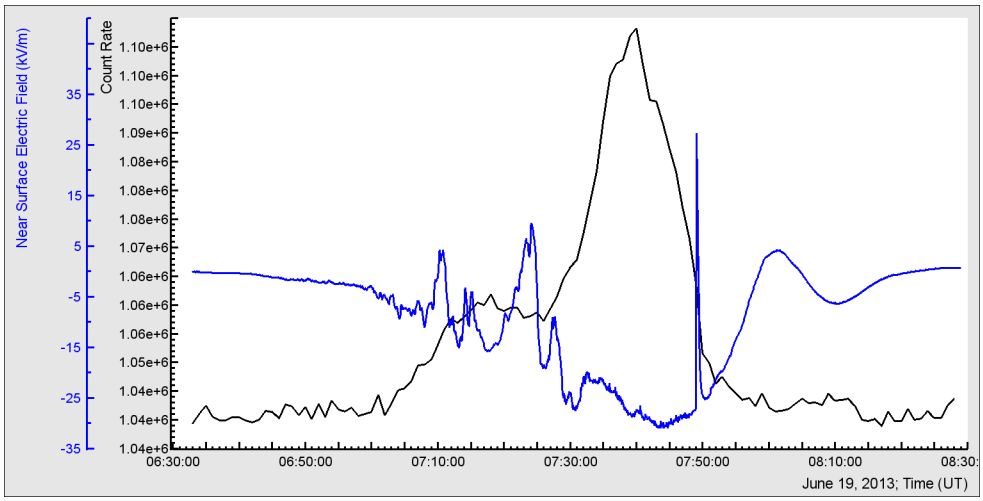

FIG. 1 (color online). TGE registered by the AMMM detector: 20 outdoor plastic scintillators; 1-minute time series of particle flux and near-surface electric field.

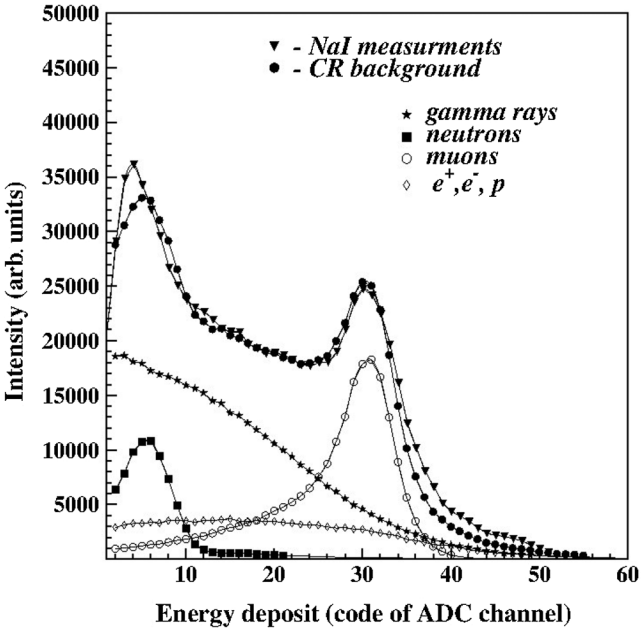

FIG. 2. Measured and simulated energy deposit spectra with the response to various species of secondary CRs.

same TGE with high significance. The large NaI crystals used for spectrometric measurements are sensitive to gamma rays and electrons from TGE as well as to different species of secondary CR. For the calibration of the spectrometer, we imitate the incident CR flux and simulate the response of the detector. The measured and simulated channel-to-channel spectra of the ADC codes are depicted in Fig. 2. We also demonstrate in the same figure the

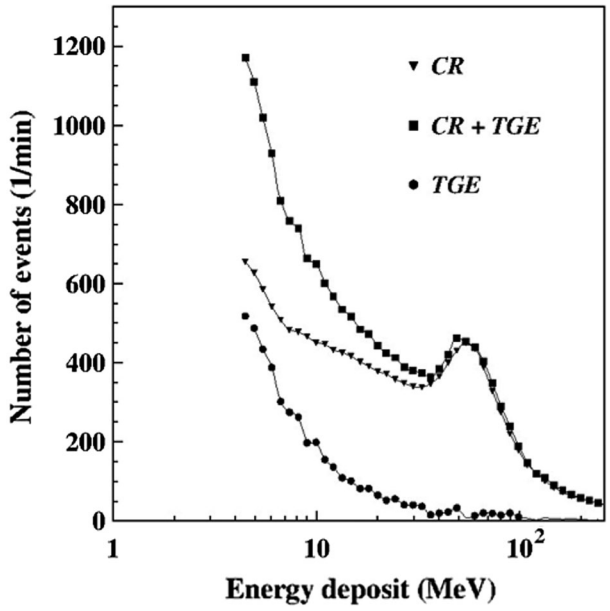

FIG. 3. Total energy deposit spectrum measured at 7:36 UT on June 19, 2013; background spectrum measured by the same NaI network 1 hour prior to TGE; and the residual TGE spectrum.

contribution of the main species of secondary cosmic rays: gamma rays, neutrons, and muons. The simulated and measured energy deposits coincide rather well; it gives us a possibility to determine the gamma ray energy as a function of the channel number. By the "muon" peak corresponding to the 30th channel of the energy deposit histogram ($\sim$ 60 MeV), we check the relation of the ADC codes to the energy deposits in MeVs.

Data acquisition electronics collects and stores 1-minute energy deposits from each of five NaI crystals. After examining the time series of particle fluxes and electric field disturbances, we determine the minute of maximum flux, and the corresponding energy deposit spectrum is compared with the background spectrum. The background spectrum was measured 1 hour prior to TGE and the mean of the 60 one-minute energy deposit spectra was used.

In Fig. 3 we can see the energy deposit spectrum (CR + TGE) measured at 7:36 UT on June 19, 2013 by five NaI crystals; the mean CR background spectrum; and the TGE spectrum obtained by the channel-to-channel subtraction of background.

III. ESTIMATION OF THE GAMMA RAY–ELECTRON RELATIVE FRACTIONS IN TGE BY STAND STACKED DETECTOR

The "STAND1" detector comprises three layers of 1-cm-thick, 1-m^2 sensitive area molded plastic scintillators (Fig. 4; see details in [23]). Light from scintillator by optical spectrum-shifter fibers is reradiated to the long-wavelength region and passed to the photomultiplier FEU-115M (PM). The maximum of luminescence is emitted at a 420-nm wavelength and the luminescence time is about 2.3 ns [33]. The tuning of the STAND1 detector consists in selections of PM high voltage and discrimination thresholds. The threshold should be chosen to guarantee both high efficiency of signal detection and maximal suppression of PM noise. Proper tuning of the detector provides $\sim$99% efficiency of charged particle detection. The data acquisition system counts and stores all coincidences of the detector channels.

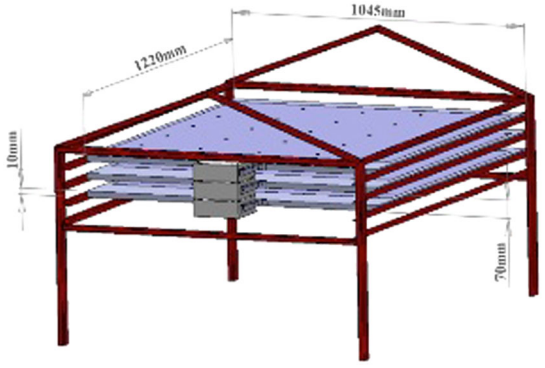

FIG. 4 (color online). STAND1 detector setup.

Coincidence "100" means that only the upper detector registers a particle. This combination registered low-energy electrons with an efficiency of ~99% (we assume that the efficiency of electron registration in the second scintillator also is 99%). We estimate the minimal energy of an electron stopping in the upper detector and giving a signal to be ~1.4 MeV; it is the lowest energy threshold among all ASEC detectors. Gamma ray detecting efficiency of this combination is about 2%. For the coincidence 010, the gamma ray detection efficiency is increased to ~3% due to creation of electron-positron pairs in the substance of the upper scintillator. Coincidence "111" means that all three layers register particles; the minimal energy of charged particles giving a signal in all three layers is ~12 MeV.

The number of particles detected by the 100 coincidence at 7:36 on June 19, 2013, was $N(100) = 32830$, and the mean value measured by the time series of STAND1 just before the TGE was 22,220; thus, the difference of 10,630 can be attributed to TGE particle flux. The number of particles detected by the 010 combination at 7:36 on June 19, 2013, was $N(010) = 25,590$, and the mean value measured by the time series of STAND1 just before the TGE was 18,100; thus, the difference of 7,490 may be attributed to TGE particle flux. By these counts, we can estimate the flux (the number of particles per square meter per minute) of electrons N_e and gamma rays N_g above the detector:

$$\begin{aligned} N(100) &= N_e p(100/e) + N_g p(100/g) \\ N(010) &= N_e p(010/e) + N_g p(010/g). \end{aligned} \tag{1}$$

p(100/e, g) and p(010/e, g) are the conditional probabilities to register electrons or gamma rays by 100 and 010 combinations. By calibration, confirmed with detector response simulations, we estimate these conditional probabilities as follows:

$$\begin{aligned} &p(100/e) = 0.99 \qquad p(100/g) = 0.02 \\ &p(010/e) = (1\text{-}p(100/e))p(100/e) = 0.0099 \\ &p(010/g) = (1\text{-}p(100/g))p(010/g) = 0,0294. \end{aligned} \tag{2}$$

Solving the system of equations (1) with coefficients (2), we readily get $N_e = 5,629$, $N_g = 252,866$ per minute per square meter. Thus, on June 19, 2013, the majority of TGE particles were gamma rays, and the fraction of electrons was $N_e/N_g \sim 2.2\%$. As we mention above, the evaluated fluxes and calculated electron–gamma ray ratio are associated with the lowest energy threshold of electron detection of ~1.5 MeV.

IV. ESTIMATION OF THE GAMMA RAY–ELECTRON RELATIVE FRACTIONS IN TGE BY CUBE DETECTOR

The Cube assembly (Fig. 5) consists of two 20-cm-thick scintillators of 0.25-m^2 area each, enfolded by 1-cm–thick, 1-m^2 area scintillators. This design ensures that no particle may hit the inside 20 cm without hitting the surrounding "veto" scintillators.

The 20-cm-thick plastic scintillators are overviewed by the photomultiplier PM-49 with a large cathode operating in a low-noise regime. Surrounding detectors (six units) are 1-cm-thick molded plastic scintillators [33].

The efficiency of neutral component detection by 1-cm-thick scintillators is ~2% and weakly depends on the energy of gamma rays. The energy losses of passing electrons and muons in 20-cm-thick plastic scintillator are ~40 MeV. Taking into account the construction material of the detector (2-mm iron tilt and 1-cm plastic scintillator), and the roof of the building (1-mm iron tilt), the electron registration energy threshold for the upper 20-cm-thick scintillator is estimated to be about 8 MeV and the bottom one ~40 MeV for the vertical flux. The obtained efficiency of gamma ray registration equals ~20% and weakly depends on energy. By using measurements from Cube's inner 20-cm-thick scintillators with and without veto signal included, we obtain the following system of linear equations:

$$\begin{aligned} N(20\text{ cm}) &= N_e p(20\text{ cm/e}) + N_g p(20\text{ cm/g}) \\ N^v(20\text{ cm}) &= N_e p^v(20\text{ cm/e}) + N_g p^v(20\text{ cm/g}), \end{aligned} \tag{3}$$

where p(20 cm/e) and p(20 cm/g) are the conditional probabilities to register electrons or gamma rays by a 20-cm scintillator. Accordingly, p^v(20 cm/e) and p^v(20 cm/g) are the conditional probabilities to register electrons or gamma rays by Cube's 20-cm upper scintillator with veto switched on. By calibration, confirmed with detector response simulations, we estimate these conditional probabilities as follows:

$$\begin{aligned} &p(20\text{ cm/e}) = 0.99 \qquad p(20\text{ cm/g}) = 0.2 \\ &p(1\text{ cm/e}) = 0.98 \qquad p(1\text{ cm/g}) = 0.02 \\ &p^v(20\text{ cm/e}) = (1\text{-}p(1\text{ cm/e}))p(20\text{ cm/e}) \\ &\qquad = (1\text{-}0.98)0.99 = 0.0198 \\ &p^v(20\text{ cm/g}) = (1\text{-}p(1\text{ cm/g}))p(20\text{ cm/g}) \\ &\qquad = (1\text{-}0.02)0.2 = 0.196. \end{aligned} \tag{4}$$

The number of particles detected by the 20-cm-thick upper scintillator at 7:36 on June 19, 2013, was $N_u = 12,920$, and the mean value measured by the Cube time series just before the TGE was 10,900; thus, the difference of 2020 can be attributed to TGE particle flux. The number of particles detected by the same detector with veto signal involved at 7:36 on June 19, 2013, was $N^v{}_u = 6245$, and the mean value measured by the appropriate time series before the TGE was 4543; thus, the difference of 1702 can be attributed to TGE particle flux. By these counts, we may estimate the flux (the number of particles per square meter per minute) of electrons N_e and gamma rays N_g above

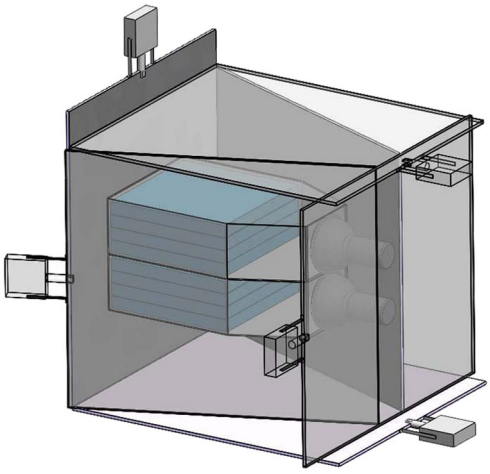

FIG. 5 (color online). Cube detector assembly design.

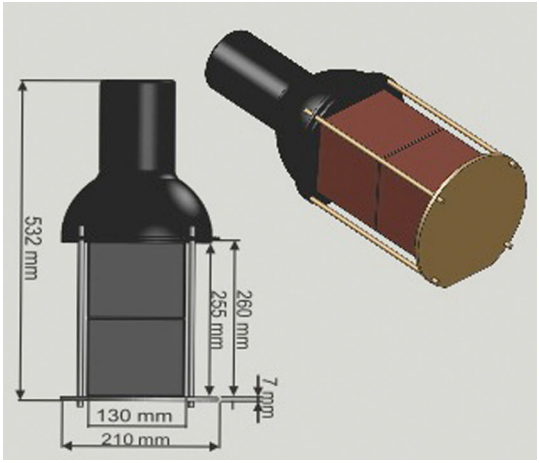

FIG. 6 (color online). NaI(Tl) crystal assembly.

the detector. Solving the system of equations (3) with coefficients (4), we readily get $N_e = 292$, $N_g = 8654$ per minute per square meter. Thus, on June 19, 2013, most of TGE particles were gamma rays; the fraction of electrons $N_e/N_g \sim 3.4\%$.

The fraction of electrons obtained by the Cube detector is larger than that obtained by the STAND1 detector because the energy threshold of the Cube detector is higher. At low energies, gamma rays are much more abundant.

V. MEASUREMENT OF THE DIFFERENTIAL ENERGY SPECTRA BY NAI CRYSTALS NETWORK

Selecting the TGE events with small electron fractions (less than 3%–4%),[2] we may neglect the electron contamination of gamma ray spectra and directly obtain the differential energy spectra by the energy deposits measured by NaI crystals.

The NaI network is located in the same experimental hall as the Cube detector; it consists of five NaI crystal scintillators in the sealed aluminum (1-mm-thick) housing. The NaI crystal is surrounded by 0.5 cm of magnesium by all sides (because the crystal is hygroscopic) with a transparent window directed to the photo-cathode of the photomultiplier tube PM-49; see Fig. 6. The large cathode of PM-49 (15-cm diameter) provides good light collection. The spectral sensitivity range of PM-49 is 300–850 nm, which covers the spectrum of NaI(Tl) emission light. The sensitive area of each NaI crystal is ~ 0.032 m^2; the total area of the five crystals is ~ 0.16 m^2; the efficiency to detect gamma rays is $\sim 80\%$. Therefore, from the peak count rate of 24,300 measured at the flux and mean background count rate of 16900 results, we calculate the TGE gamma ray flux of 57,812 per square meter per minute.

[2]The accuracy of the electron fraction determination by Cube and STAND1 detectors was estimated to be $\sim 1.5\%$.

After determining the fraction of electrons and gamma rays in TGE flux, we select several recent TGE events containing small proportions of electrons to investigate the differential gamma ray spectra measured by the network of NaI crystals. Gamma ray spectra presented in Figs. 7–11 were obtained by the summed intensity measured by five NaI crystals. The 1-minute background spectrum was obtained by averaging the 1-hour data (60 energy release histograms) measured before the enhancement of secondary cosmic ray flux. The TGE 1-minute spectrum was obtained by averaging 3–4 minute data around the flux maximum minute. On Figs. 7–11, the residual (gamma ray) spectra are placed.

For the channels of 3–4 MeV, NaI crystals underestimate the intensity due to lower efficiency of gamma ray detection near the electronic threshold. For the highest energies

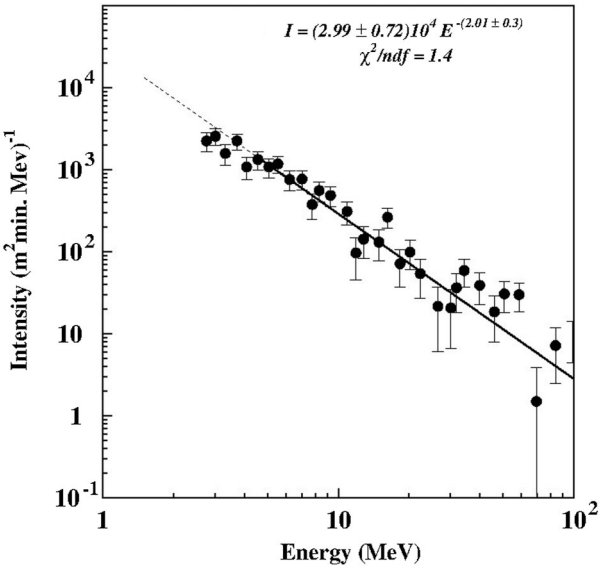

FIG. 7. Differential gamma ray energy spectrum; TGE of October 7, 2012; peak time at 14:09; exposition of 3 minutes.

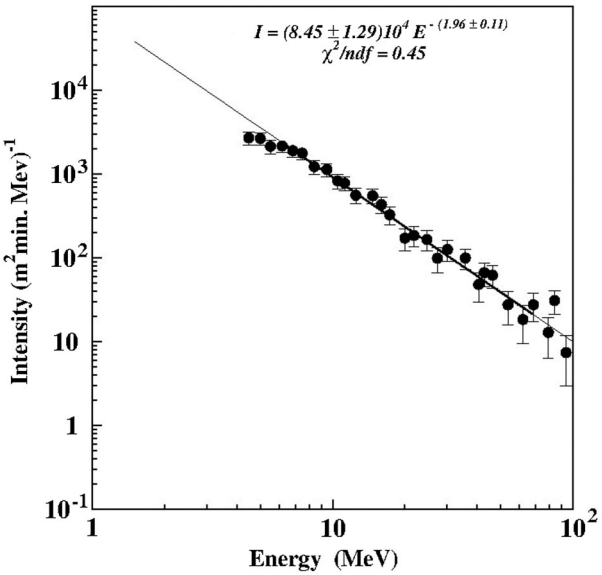

FIG. 8. Differential gamma ray energy spectrum; TGE of May 12, 2013; peak time at 06:36; exposition of 3 minutes.

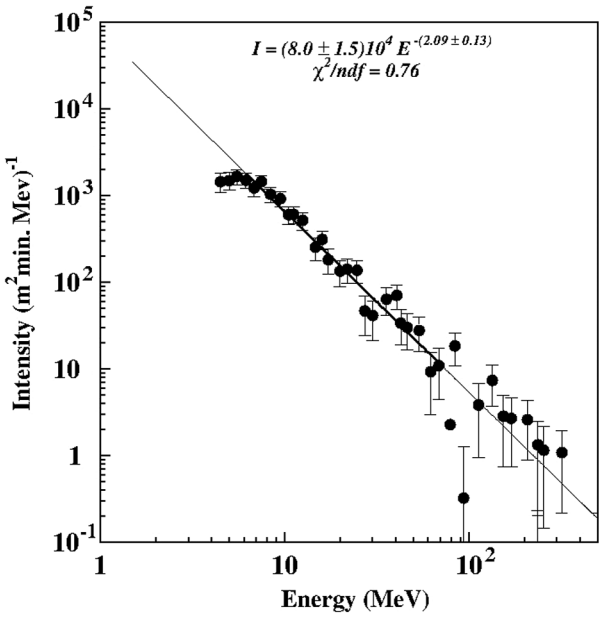

FIG. 9. Differential gamma ray energy spectrum; TGE of May 15, 2013; peak time at 12:30; exposition of 4 minutes.

(above 60 MeV), gamma rays may not deposit their whole energy in the crystal. The GEANT simulations were used to study these effects and appropriate corrections were introduced. Because of the high intensity of the June 19 TGE, it was possible to measure energy spectra separately by all five NaI crystals. As one can see in Fig. 12, spectra measured by all five NaI crystals are very close to one another. At energies above 30 MeV, low statistics lead to a larger variance of the spectra channels measured by the

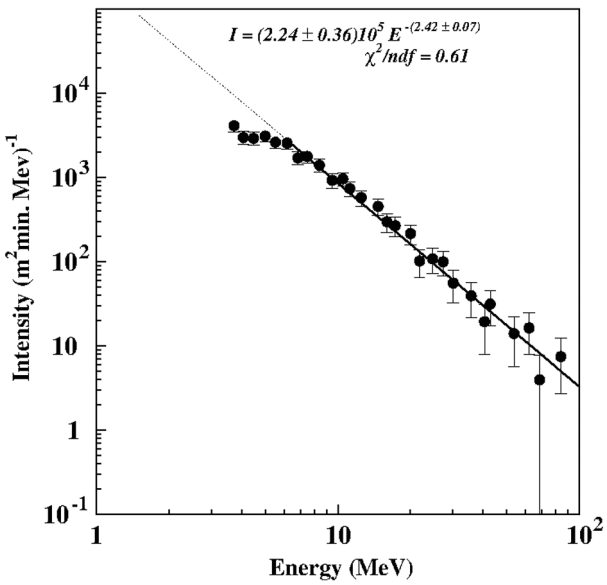

FIG. 10. Differential gamma ray energy spectrum; TGE of June 9, 2013; peak time at 21:47; exposition of 3 minutes.

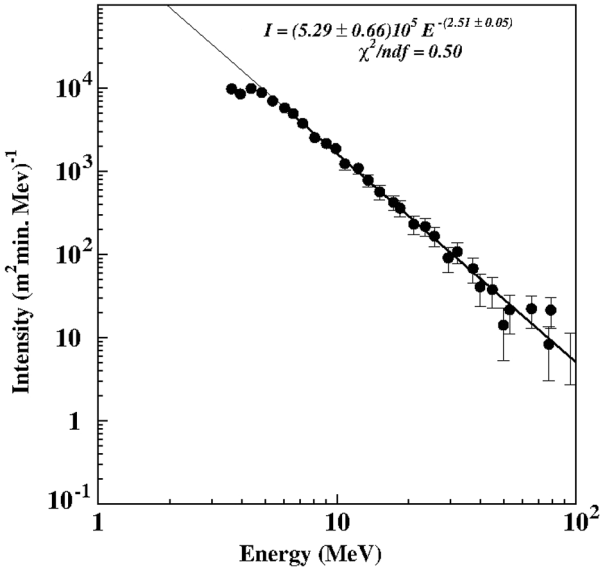

FIG. 11. Differential gamma ray energy spectrum; TGE of June 19, 2013; peak time at 07:36; exposition of 4 minutes.

individual crystals. However, as we can see in Fig. 11, the error bars of the overall spectra are rather small.

VI. CHECKING THE THRESHOLD OF ARAGATS PARTICLE DETECTORS BY MEASURED GAMMA RAY INTEGRAL ENERGY SPECTRA

The ultimate check of the energy spectra measurements with NaI crystals will be an independent estimate of the particle flux by other ASEC detectors. The energy spectrum of gamma rays obtained by the NaI detector was compared with the detector response of the STAND1,

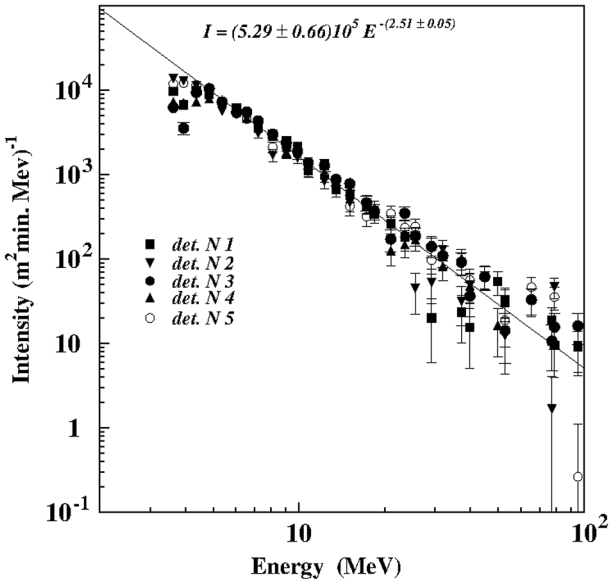

FIG. 12. Differential energy spectra of gamma rays measured by all five crystals of NaI detectors at 7:34–07:37 on June 19, 2013. The solid line represents the power law spectrum fitted by the sum of all five crystals.

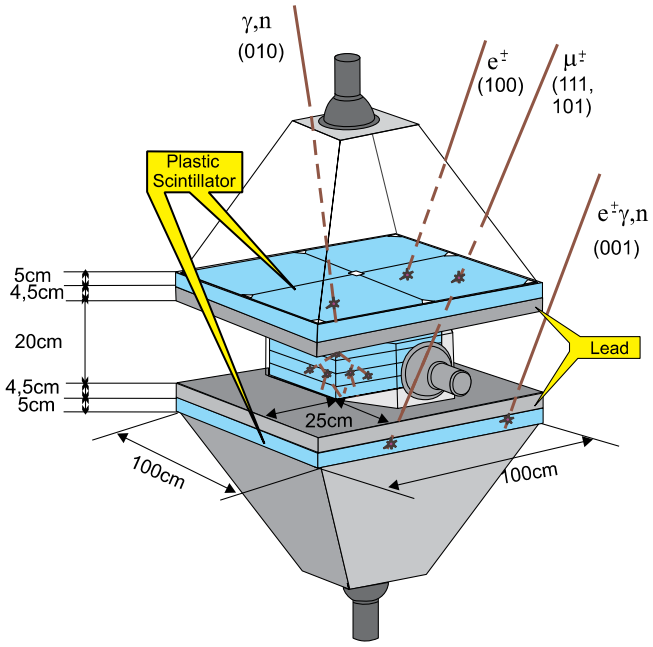

FIG. 13 (color online). SEVAN network basic measuring unit.

Cube, and SEVAN detectors. The integral spectrum of the NaI crystals on June 19, 2013, equals 57,812 per square meter per minute. The integral spectrum of gamma rays measured by the STAND1 detector was 252,870 per square meter per minute. The number of particles detected by the 20-cm-thick Cube bottom scintillator was $N_b = 11,420$, and the mean value measured by the Cube time series just before the TGE was 9642; thus, the difference of 1702 and flux of 31,424 gamma rays per square meter per minute can be attributed to TGE gamma ray flux.

The basic detecting unit of the SEVAN (Space Environmental Viewing and Analysis Network [34]) module (see Fig. 13) is located in the MAKET building 20 m apart from the outdoor STAND1 detector. The number of particles detected by the 20-cm-thick SEVAN middle scintillator at 7:36 on June 19, 2013, was $N = 8269$, and the mean value measured by the SEVAN time series just before the TGE was 7692; thus, the difference of 577 and flux of 11,540 gamma rays per square meter per minute[3] can be attributed to TGE gamma ray flux (electrons of MeV energies will be efficiently filtered in the detector material). Analogically, we estimate the integral energy spectrum measured by the upper scintillator of STAND1 detector, the bottom Cube detector, and the NaI detector itself. Thus, we have several integral energy spectrum measurements to be checked with the interpolated differential energy spectrum depicted in Fig. 11.

The spectrum shown in Fig. 14 by the solid line was obtained by integration of the differential spectrum measured by five NaI crystals, shown in Fig. 11. From the projection of the integral spectra of different detectors on the x axes, we readily obtain the thresholds of these detectors to register gamma rays. The integral spectrum measured by the STAND1 detector corresponds to a threshold energy of ~1.4 MeV; the NaI threshold corresponds to

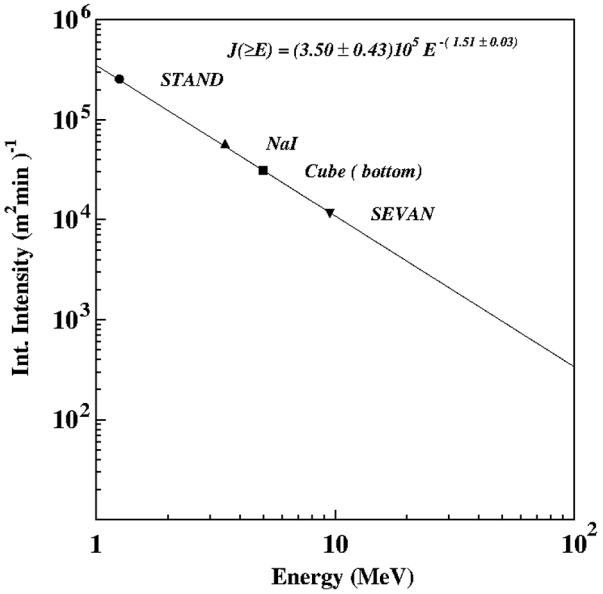

FIG. 14. Integral gamma ray energy spectrum; TGE of June 19, 2013; peak time at 07:36.

[3]The surface of SEVAN's middle scintillator is 0.25 m^2 and efficiency to detect gamma rays ~20%.

TABLE I. Parameters of five differential energy spectra of gamma rays in TGEs with small electron contamination and parameters of the two largest TGE events.

Event date	Peak time	A $(m^2\ min\ MeV)^{-1}$	$-\gamma$	Peak significance (N of σ)	TGE duration (min)
10/7/2012[a]	14:09	$(2.99 \pm 0.72) \times 10^4$	2.01 ± 0.3	11	15
5/12/2013[a]	06:36	$(8.45 \pm 1.29) \times 10^4$	1.96 ± 0.11	23	14
5/15/2013[a]	12:30	$(8.0 \pm 1.5) \times 10^4$	2.09 ± 0.33	22	12
6/9/2013[a]	21:47	$(2.24 \pm 0.36) \times 10^5$	2.42 ± 0.07	34	9
6/19/2013[a]	07:36	$(5.29 \pm 0.66) \times 10^5$	2.51 ± 0.05	36	74
9/19/2009[b]	22:47	$(5.2 \pm 2.4) \times 10^7$	3.4 ± 0.25	465	13
10/4/2010[b]	18:23	$(4.2 \pm 2.1) \times 10^7$	3.3 ± 0.02	164	12

[a]Measured by the network of NaI crystals differential energy spectrum; peak significance and duration measured by the NaI network in the energy range 4–100 MeV.
[b]Differential energy spectrum recovered by the ASNT energy releases (60-cm-thick scintillators) in the energy range 10–100 MeV; peak significance and duration measured by 1-m^2, 5-cm-thick plastic scintillator.

~3 MeV, the Cube bottom scintillators to ~4 MeV, and the SEVAN middle scintillator (below 4.5 cm of lead) to ~10 MeV.

VII. DISCUSSION AND CONCLUSIONS

The parameters of five gamma ray differential energy spectra measured by the NaI network, as well as parameters of the spectra of the two largest TGEs that occurred in 2009 and 2010, are depicted in Table I. We post in the table successively the TGE date, the intensity of 1-MeV gamma rays (A, the multiplicator of power law energy spectra), the power law spectral index ($-\gamma$), the significance of the peak at its maximal flux minute (in number of standard deviations from the mean value of count rate), and the duration of the TGE.

According to our model [35], the origin of TGE is a radiating region in the bottom of the cloud connected to the transient lower positive charged region that forms a lower dipole with the main negative charge region in the middle of the cloud. Intensive electrical field between these layers accelerates electrons downward and gives birth to two processes:

The relativistic runaway electron avalanche process sustaining electron and gamma ray fluxes up to ten times or more above background cosmic ray intensity;

The modification of CR energy spectra process, prolonging the live time of electrons in thunderstorm atmosphere; those in turn radiate additional gamma rays.

TGEs usually occurred during negative near-surface electrical field varying from −10 to −30 kV/m (see Fig. 1); electric field in the thundercloud may be much more strong, reaching values of ~200 kV/m. For releasing the RREA process at a 4000–5000 m height, a minimum 170 kV/m strength of electric field is required (the so-called threshold electric field [3]). Due to multiplication of electrons in the avalanche, the number of particles in the TGE may be very large, exceeding the cosmic ray background tens of times (see the last two rows of Table I and details in [1,2]). Simultaneously, the absolute value of the power law spectral index will be big, reflecting the fast attenuation of RREA electron spectra. Consequently, the

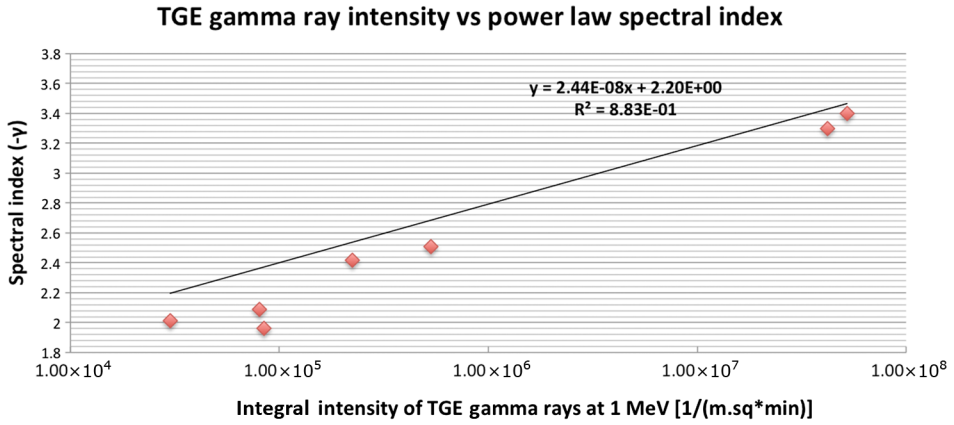

FIG. 15 (color online). Correlation of absolute value of power law spectral index and event intensity.

energy spectrum of RREA-TGE gamma rays also should be steep (see the last four rows of Table I; spectral indices equal -2.42, -2.51, -3.3 and -3.4).

If electric field is below the RREA threshold, only the MOS process will take place. The MOS process does not demand very large electric fields and enhances particle flux only by a few percent; however, it specifies a long tail of the gamma ray energy spectra extending up to 100 MeV [12]. A gamma ray spectrum extending up to 100 MeV also was obtained by facilities of the gamma ray observatory on board the AGILE satellite [36]. The MOS-TGE flux is weaker than the RREA-TGE flux and mainly consists of the additional gamma rays. The spectral indices of small TGEs posted in the first three rows of Table I are equal to -2.01, -1.96, -2.09, in good coincidence with spectra measured by the Japanese group [15,28].

The positive correlation of the absolute value of the power law spectral index and event intensity (see Fig. 15) proves the existence of distinct RREA and MOS scenarios of TGE.[4]

Thus, we may conclude that the measured energy spectra of TGE gamma rays points toward two main mechanisms of the TGE origin: the runaway process and the modification of electron energy spectra in thunderstorm atmospheres.

ACKNOWLEDGMENTS

This work was partly supported by Armenian government grants. The authors thank Karen Avagyan, Karen Arakelyan, and Arthur Reymers for assembling the NaI crystal network. The authors are grateful to Levon Vanyan for discussing different scenarios of TGE origination.

[4]The TGE origin may be only MOS process, if electric field in thundercloud is below the breakeven field value; if it is larger—both MOS and RREA processes may give rise to TGE.

[1] A. Chilingarian, A. Daryan, K. Arakelyan, A. Hovhannisyan, B. Mailyan, L. Melkumyan, G. Hovsepyan, S. Chilingaryan, A. Reymers, and L. Vanyan, Phys. Rev. D **82**, 043009 (2010).
[2] A. Chilingarian, G. Hovsepyan, and A. Hovhannisyan, Phys. Rev. D **83**, 062001 (2011).
[3] J. R. Dwyer, D. M. Smith, and S. A. Cummer, Space Sci. Rev. **173**, 133 (2012).
[4] C. T. R. Wilson, Math. Proc. Cambridge Philos. Soc. **22**, 534 (1925).
[5] A. V. Gurevich, G. M. Milikh, and R. A. Roussel-Dupre, Phys. Lett. A **165**, 463 (1992).
[6] L. P. Babich, E. N. Donskoi, I. M. Kutsyk, and A. Yu. Kudryavtsev, Phys. Lett. A **245**, 460 (1998).
[7] J. R. Dwyer, Geophys. Res. Lett. **30**, 2055 (2003).
[8] N. S. Khaerdinov, A. S. Lidvansky, and V. B. Petkov, Atmos. Res. **76**, 346 (2005).
[9] Y. Muraki *et al.*, Phys. Rev. D **69**, 123010 (2004).
[10] L. I. Dorman and I. V. Dorman, Adv. Space Res. **35**, 476 (2005).
[11] A. S. Lidvansky and N. S. Khaerdinov, Izv. Ross. Akad. Nauk, Ser. Fiz. **71**, 1052 (2009) [Bulletin of the Russian Academy of Sciences: Physics **71**, 1052 (2009)].
[12] A. Chilingarian, B. Mailyan, and L. Vanyan, Atmos. Res. **114–115**, 1 (2012).
[13] A. Chilingarian, N. Bostanjyan, and L. Vanyan, Phys. Rev. D **85**, 085017 (2012).
[14] A. Chilingarian, N. Bostanjyan, T. Karapetyan, and L. Vanyan, Phys. Rev. D **86**, 093017 (2012).
[15] H. Tsuchiya, K. Hibino, and K. Kawataetal, Phys. Rev. D **85**, 092006 (2012).
[16] L. P. Babich, E. I. Bochkov, A. N. Zalyalov, and I. M. Kutsyk, Pis'ma Zh. Eksp. Teor. Fiz. **97**, 333 (2013) [JETP Lett. **97**, 333 (2013)].
[17] A. S. Lidvansky and N. S. Khaerdinov, Izv. Ross. Akad. Nauk, Ser. Fiz. **73**, 415 (2009) [Bulletin of the Russian Academy of Sciences: Physics **73**, 415 (2009)].
[18] J. R. Dwyer, M. M. Schaal, E. Cramer, S. Arabshahi, N. Liu, H. K. Rassoul, J. D. Hill, D. M. Jordan, and M. A. Uman, J. Geophys. Res. **117**, A10303 (2012).
[19] A. V. Germanenko, Yu. V. Balabin, E. V. Vashenyuk, B. B. Gvozdevsky, and L. I. Schur, Astrophys. Space Sci. Trans. **7**, 471 (2011).
[20] A. Chilingarian *et al.*, J. Phys. G **29**, 939 (2003).
[21] A. Chilingarian *et al.*, Nucl. Instrum. Methods Phys. Res., Sect. A **543**, 483 (2005).
[22] K. Arakelyan, K. Avakyan, A. Chilingarian, A. Daryan, L. Melkumyan, D. Pokhsraryan, and D. Sargsyan, J. Phys. Conf. Ser. **409**, 012223 (2013).
[23] K. Avakyan, K. Arakelyan, A. Chilingarian, A. Daryan, L. Kozliner, B. Mailyan, G. Hovsepyan, D. Pokhsraryan, and D. Sargsyan, J. Phys. Conf. Ser. **409**, 012218 (2013).
[24] A. Chilingarian, T. Karapetyan, and L. Melkumyan, Adv. Space Res. **52**, 1178 (2013).
[25] S. Chilingaryan, A. Beglarian, A. Kopmann, and S. Vöcking, J. Phys. Conf. Ser. **219**, 042034 (2010).
[26] A. S. Lidvansky and N. S. Khaerdinov, Izv. Ross. Akad. Nauk, Ser. Fiz. **73**, 418 (2009) [Bulletin of the Russian Academy of Sciences: Physics **73**, 418 (2009)].
[27] H. Tsuchiya *et al.*, Phys. Rev. Lett. **99**, 165002 (2007).
[28] H. Tsuchiya *et al.*, J. Geophys. Res. **116**, D09113 (2011).
[29] G. J. Fishman *et al.*, Science **264**, 1313 (1994).
[30] D. M. Smith, L. I. Lopez, R. P. Lin, and C. P. Barrington-Leigh, Science **307**, 1085 (2005).
[31] M. S. Brigs *et al.*, J. Geophys. Res. **115**, A07323 (2010).

[32] A. Chilingarian, B. Mailyan, and L. Vanyan, Astropart. Phys. **48**, 1 (2013).

[33] G. Britvich, V. G. Vasil'chenko, V. N. Kirichenko, S. I. Kuptsov, V. G. Lapshin, A. P. Soldatov, A. S. Solov'ev, V. I. Rykalin, S. K. Chernichenko, and I. V. Shein, Instrum. Exp. Tech. **45**, 644 (2002); G. Britvich *et al.*, http://www.ihep.su/.

[34] A. Chilingarian and A. Reymers, Ann. Geophys. **26**, 249 (2008).

[35] A. Chilingarian and R. Mkrtchyan, Phys. Rev. D **86**, 072003 (2012).

[36] M. Tavani *et al.*, Phys. Rev. Lett. **106**, 018501 (2011).